Operation Control for Improving Energy Efficiency of Shipboard Microgrid including Bow Thrusters and Hybrid Energy Storages

Xiao, Zhao Xia; Li, Huai Min; Fang, Hong Wei; Guan, Yu Zhe; Liu, Tao; Hou, Lucas; Guerrero, Josep M.

Published in:
IEEE Transactions on Transportation Electrification

DOI (link to publication from Publisher):
10.1109/TTE.2020.2992735

Publication date:
2020

Document Version
Accepted author manuscript, peer reviewed version

The final version of record is available at http://dx.doi.org/10.1109/TTE.2020.2992735

Operation Control for Improving Energy Efficiency of Shipboard Microgrid including Bow Thrusters and Hybrid Energy Storages

Zhao-xia Xiao, Huai-min Li, Hong-wei Fang, Senior member, *IEEE*, Yu-zhe Guan, Tao Liu, Lucas Hou, Josep M. Guerrero, Fellow, *IEEE*

***Abstract*—The frequent start/stop operation of a bow thruster presents a high pulsating power demand in shipboard microgrids while reducing the fuel efficiency of the diesel engines, which may induce potential instabilities. In this paper, a hybrid energy storage system, including batteries and ultra-capacitors, is connected to the DC bus of the thruster driver, and a hierarchical controller is proposed for the bidirectional DC/DC converters that interface storages thus providing the following functions: (1) the diesel-generator sets provide the required average power to the bow thruster; (2) the batteries smooth the active power fluctuations; and (3) the ultra-capacitors provide the pulsating active power due to the slow charging response of batteries. A V-I droop control and high/low-pass filters are used inside the primary controller to proper power sharing between storages in different time-scales. The secondary controller is developed to ensure the power from the diesel-generator sets to the bow thruster being equal to the required average power. Simulation results shows this control scheme can effectively reduce the capacity of diesel generator sets and batteries, and can improve the fuel consumption efficiency. When the thruster machine operates as a generator during fast breaking, the hybrid energy storage can absorb the braking energy.**

***Index Terms*—Shipboard Microgrid, Bow Thruster, Hybrid Energy Storage, Coordinated Control, V-I Droop, Feedback Generation**

I. NOMENCLATURE

Parameter	*Description*
SFC	Specific Fuel Consumption [g/kWh]
f_{PL}	Load power fluctuation frequency [Hz]
f_{cut}	High / low pass filter cutoff frequency [Hz]
V_{dc}	DC bus voltage [V]
V_{dc}^{*}	DC bus reference voltage [V]
δV	Compensation voltage [V]
P_L	Load power [kW]
V_0	No-load voltage reference value [V]
P_B	Batteries active power [kW]
P_{UC}	Ultra-capacitors active power [kW]
P_{DG}	Diesel generator active power [kW]
Q_{DG}	Diesel generator reactive power [Var]
V_m	Phase-voltage peak value of the synchronous generator [V]
ω	High and low pass filter cutoff angular frequency[rad/s]
ω_e	Electrical angular speed [rad/s]
L_{ac}	AC-side equivalent inductance [mH]
I_{dc}	Output DC current of the diesel generator [A]
i_{L1}	Inductive current in a battery DC/DC converter [A]
i_{L2}	Inductive current in an Ultra-capacitors DC/DC converter [A]
i_{L1a}	Inductance current of a phase branch in battery DC/DC converter [A]
i_{L1b}	Inductance current of b phase branch in battery DC/DC converter [A]
i_{L1c}	Inductance current of c phase branch in battery DC/DC converter [A]
i_{sq}	q components of the stator current of bow thruster machine [A]
i_{sd}	d components of the stator current of bow thruster machine [A]
ω_r	Rotor angular speed of bow thruster machine[rad/s]
λ_r	Rotor flux linkage of bow thruster machine [Wb]
n_r	Rotor speed of bow thruster machine [rpm]
L_M	Mutual inductance between stator and rotor of bow thruster machine [mH]
L_{lr}	Rotor leakage inductance of bow thruster machine [mH]
r_r	Rotor resistance of bow thruster machine [Ω]
p	Differential operator [-]
i_{sd}	Stator d-axis current of bow thruster machine .
T_e	Electrical torque of bow thruster machine [N·m]
T_L	Load torque of bow thruster machine [N·m]
θ	Rotor flux position angle of bow thruster machine [°]
$\hat{i}_L$	State variables of the inductor current of DC-DC converters[A]
I_L	Steady state current in the inductor of DC-DC converters [A]
$\hat{v}_{dc}$	State variables of the DC bus voltage [V]
$\hat{u}_B$	State variables of the battery voltage [V]
D	Steady-state PWM duty ratio of DC-DC converters [-]

This work was supported by the Tianjin Science and Technology Support Program Key Project and National Natural Science Foundation of China (17JCZDJC31300,19JCZDJC32200, 19JCQNJC03600, 51977149, 51807139, and 51877148). This work was also supported by VILLUM FONDEN under the VILLUM Investigator Grant (no. 25920): Center for Research on Microgrids (CROM).

Zhao-xia Xiao, **Huai-min Li**, **Yu-zhe Guan** and **Tao Liu** are with Tianjin Key Laboratory of Advanced Electrical Engineering and Energy Technology, Tiangong University, Tianjin, 300387, P. R. China. Email:xiaozhaoxia@tiangong.edu.cn

Hong-wei Fang is with School of Electrical and Information Engineering, Tianjin University, Tianjin 300072, P. R. China. Email:hongwei_fang@tju.edu.cn

Lucas Hou is in RENergy Electric Tianjin Ltd, Tianjin, 300385, P. R. China. Email:lj.hou@relectric.cn

Josep M. Guerrero is in Center for Research on Microgrids (CROM), Department of Energy Technology, Aalborg University, 9220 Aalborg East, Denmark. E-mail: joz@et.aau.dk.

The final version of record is available at http://dx.doi.org/10.1109/TTE.2020.2992735

$\hat{d}$	State variables of the duty cycle of DC-DC converters [-]
$\hat{i}_o$	State variables of the output current of DC-DC converters [A]
x	State variables of state-space equation[-]
y	Input variables of state-space equation [-]
K	Droop gain of the outer loop V-I droop controller[-]
K_p	Proportional of the inner current loop PI controller[-]
K_i	Integral coefficient of the inner current loop PI controller[-]
K_{P_DG}	Droop gain between active power and rotor speed of diesel generator [kW]
K_{Q_DG}	Droop gain between reactive power and terminal voltage of the diesel generator [kVar]
T_1	Time constant of speed regulator[-]
T_2	Time constant of excitor[-]
ω_{DG}	Diesel engine rotation speed[rad/s]
i_{L1ref}	Reference value of inductive current for battery DC/DC converter [A]
i_{L2ref}	Reference value of inductive current for ultra-capacitors DC/DC converter [A]
r	Virtual resistance [Ω]
r_1	Virtual impedance of Battery DC/DC converter controller [Ω]
r_2	Virtual impedance of UCs DC/DC converter controller[Ω]
m	Power droop coefficient[-]
P_{con}	Output power of the DC/DC converter [kW]
V_{nom}	DC bus rated voltage[V]
C	Capacitance of DC/DC converter [F]
L	Inductance of DC/DC converter [H]

II. INTRODUCTION

Increasing concerns on environmental issues and fuel economy have forced the maritime industry to pursue the solutions of low emission and fuel efficiency [1], [2]. In the past, the conventional propulsion drivetrains were mostly mechanical and relatively isolated from the shipboard power system. In the 1990s, power electronic converters made a breakthrough that they enabled electrification of propulsion systems through variable speed drives in marine vessels [3]. Electric propulsions promote the unified power supply mode of the shipboard power system and make the concept of the integrated shipboard power system. Nowadays, the shipboard power system has complex network architectures and multifarious power-electronic interfaced loads and sources [4]-[7].

Shipboard power system becomes more or less similar to land-based microgrids. The common characteristics between the shipboard microgrids and land-based microgrids include islanded operation, increased use of power electronic converters and network architectures. Therefore, technologies developed for islanded land-based microgrids can be extended for ship microgrids as well [8]. Nevertheless, there are also some differences between them: 1) wind, waves, and ocean currents pose challenges to the stability, reliability, and survivability of the shipboard power system; 2) the generation source of shipboard microgrid is mainly diesel-generator set; 3) large dynamic propulsion and pump loads account for about 70% of the total load power; 4) the volume and weight requirements of the ship's power equipment are relatively high. Therefore, the coordinated control of shipboard microgrid requires to consider both stability and energy efficiency based on various operation scenarios and missions.

With maneuverability improvement of a ship, bow thrusters are gradually applied in some offshore vessels and ferries. Usually, there are two propellers embedded in the bottom of the ship named bow thrusters, which generates the lateral thrust to enhance the maneuverability and flexibility of the ship for dynamic positioning, docking, and undocking. In the dynamic positioning application, bow thruster will typically be ramping from 1,000 rpm in one direction to 1,000 rpm in the other direction in less than 10 seconds. Thus, the thruster machine usually starts with huge peak power in a very short interval time and generates power during fast braking. Therefore, it belongs to the short-term pulse loads, which may induce the following problems [9]:

1) Pulse loads have a high dynamic response demands during their operation, and the diesel-generator set cannot follow to the load power change.

2) The high transient power demand of bow thrusters may cause the frequency deviation and voltage fluctuation in the shipboard microgrid.

3) The fuel consumption efficiency of diesel-generator sets will be reduced since its output power keeps changing.

4) When the thruster machine operates as a generator during fast braking, braking resistor absorbs energy and causes waste.

Regarding the operation characteristics of a bow thruster, the energy storage is investigated to use in the main bus or the DC bus of driver chain including batteries, ultra-capacitors, and flywheel. Comprehensive analysis of different energy storage technologies is conducted and Table 1 provide the matrices to clearly show the positions of different energy storage performance and characteristics [10]. In [11], the hybrid fuel cell with ultra-capacitors supply for the bow thruster and the fast response of the ultra-capacitors can satisfy the initial state of high torque constraints. In (Kulkarni 2009), flywheels have been explored to supply for the pulse power loads on the drilling platform. In [12], a hybrid energy storage system configuration, namely, batteries combined with flywheels, reduces load fluctuations and performs comparative research with the battery and ultra-capacitor. In [13], the ultra-capacitors are connected in parallel to the three-phase inverter of the bow thruster, providing a large current when the propeller is frequently started during the docking process for several tens of seconds. In [14], hybrid energy storage is used to smooth the load power fluctuations of the shipboard microgrid. With multiple time-scale characteristics of the propulsion load power, the complementary characteristics of batteries and ultra-capacitors have been investigated to suppress load fluctuations [15], [16].

TABLEI PERFORMANCE AND CHARACTERISTICS OF DIFFERENT ENERGY STORAGES.

Storage Technology	Energy Efficiency(%)	Power Density (W/kg)	Energy Density (Wh/kg)	Life Time (cycles)	Deployment Time	Applications
Lead-acid batteries	70-90	500-1000	30-50	200-300	1 to 5 seconds	Automobiles, Forklifts and large uninterruptible power supply (UPS) systems

The final version of record is available at http://dx.doi.org/10.1109/TTE.2020.2992735

Lithium-ion batteries	87-94	150-2000	80-170	10^3-10^4	5 to 20 milliseconds	Residential storage systems, Voltage control, Load levelling, Peak shaving
Nickel Cadmium (NiCd) batteries	-		45-80	1500	-	Two-way radios, Emergency medical equipment and power tools
Air-Energy Storage	60-70	-	30-60	30 years	3 to 10 min	Voltage control, Load levelling, Peak shaving, Standing Reserve
Flywheel Energy Storage	85-87	1500-5000	5-50	10^6	about 10 milliseconds	Primary Frequency control, Voltage control, Peak shaving, UPS
Ultra-Capacitors	90-94	1000-10000	<50	10^6	<10 milliseconds	Primary Frequency control, Voltage control, Peak shaving, UPS

In this paper, hybrid energy storage including batteries and ultra-capacitors connected to the DC side of the bow thruster driver is proposed. According to the fuel consumption characteristics of diesel engine and the complementary characteristics of batteries and ultra-capacitors, the diesel-generator sets provide the average power for the bow thruster, the batteries and ultra-capacitors operate as an energy buffer in different time scale. This method reduces the impact of the instantaneous starting current on the shipboard microgrid, increases the fuel consumption efficiency of the diesel engine and decrease the capacity of diesel generator sets and batteries. At the same time, when the bow thruster operates as a generator when fast braking, the energy storage can replace the DC-bus resistor and absorb the braking energy generated [1]. Hierarchical control is applied to the interleaved three-phase bidirectional DC/DC converters of storages, where a V-I droop and high-pass and low-pass filters are used to the primary controller to realize the parallel of the storages and load power-sharing in different time scale. The secondary controller is to ensure the output power from the diesel-generator sets to the bow thruster equal to the required average power. The main goals in this paper are proposed as follows :

*1)*Solve that the diesel generator sets cannot track the rapid power change of the bow thruster by using hybrid energy storage.

*2)*Improve the fuel consumption efficiency and reduce the capacity of diesel-generator sets.

*3)*Absorb the fast-braking energy of the thruster machine and avoid energy waste.

This paper is organized as follows. Section II introduces the structure of the shipboard microgrid and gives the coordinated control principle between diesel-generator sets and hybrid energy storages. Section III describes the hierarchical control including the primary and secondary control layer. The controller parameter margin is analyzed in Section IV. In Section V, the simulation model and simulation results are analyzed. Section VI concludes this paper.

III. PRINCIPLE OF COORDINATED CONTROL

All-electric ships (AES) are generally composed of diesel generator sets, electric propulsion systems, electric thruster systems, and other service loads, as shown in Fig. 1.

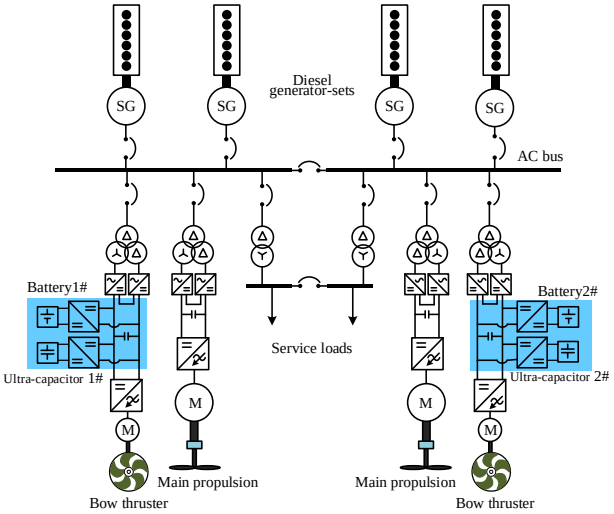

Fig. 1. Structures of the shipboard microgrid.

The shipboard microgrid generally uses a single bus segmentation distribution topology. 12-pulse rectification is generally used in the terminal of diesel synchronous generator to reduce harmonics. The bow thruster is driven by an inverter with the speed regulation function by the frequency conversion. In order to improve the fuel efficiency of diesel generator sets and reduce the impact of power fluctuation of the bow thruster on a shipboard microgrid, this paper proposes that bow thruster is powered by diesel generator sets and a hybrid energy storage system including the batteries and ultra-capacitors. And when the thruster is fast braking, the bow thruster machine operates as the generator and the braking energy can be fed back to the energy storage system. Based on the possible feedback energy of the bow thruster, the battery capacity is fixed and the ultra-capacitor capacity is determined by the power ramp and the peak value of the bow thruster. The batteries are interfaced by interleaved three-phase bidirectional DC/DC converters and the ultra-capacitors are also interfaced by interleaved three-phase bidirectional DC/DC converters due to it can reduce the impact of the large start current of bow thruster on the power electronics switch. At the same time, a coordinated control method for multiple supply sources is presented.

The specific fuel consumption (SFC) curves have qualitative behavior in Fig. 2 (a). When the diesel engine runs at a fixed speed and wants to maintain the optimal fuel utilization rate, it must maintain a fixed generation power of about 80-90% rated power.

The optimal output power-speed characteristics of the diesel engine are shown in Fig. 2 (b). When the output power of the diesel generator increases, it is necessary to increase the diesel engine speed (namely the mechanical torque is maintained at the rated torque) to improve the operation fuel efficiency. While the characteristics between the active power and the speed of a synchronous generator is a kind of natural droop curve, it is opposite to the optimal power-speed characteristics of the diesel engines.

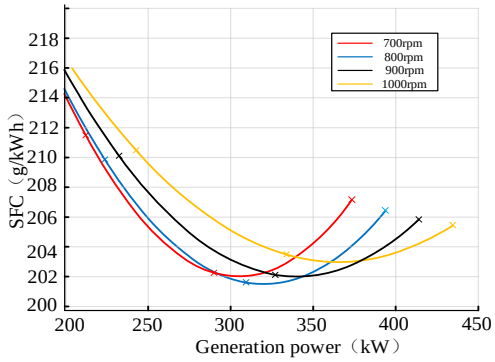

(a)Relationship between specific fuel consumption, output power and rotation speed of diesel engine.

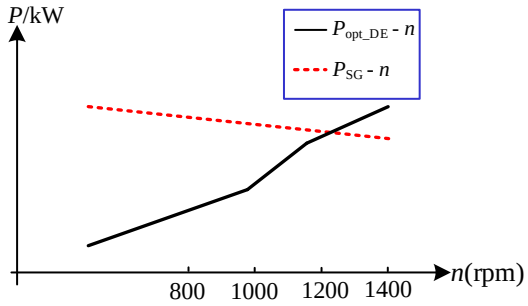

(b)The optimal power-speed characteristics of the diesel engine and the power-speed characteristics of synchronous generator.

Fig. 2. The characteristics of specific fuel consumption, output power, and rotation speed.

As shown in Fig. 3, the power demand of the bow thruster is an approximate pulse power. According to Fig.2(b), a coordinated power supply by diesel generators, batteries and ultra-capacitors is provided. When the power demands of the bow thruster change, the diesel generator sets will provide the average power for the bow thruster, and the batteries and the ultra-capacitors are used to maintain the power balance by charging and discharging. Since the characteristics of the high energy density of the battery and high-power density of ultra-capacitors (UCs), the fluctuated power of bow thruster is mainly provided by the battery, and the ultra-capacitors provides the impulse power for the start and brake of the bow thruster. That is, the ultra-capacitors handle the high-frequency fluctuated power while the batteries deal with low-frequency fluctuated power of the bow thruster.

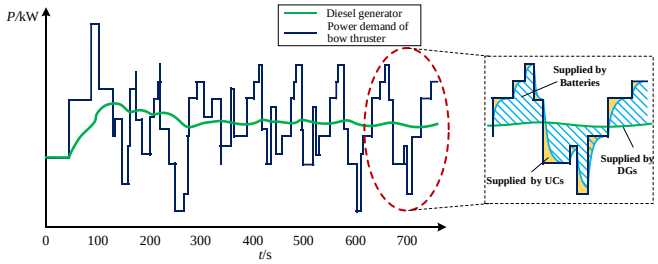

Fig. 3. Power demand of bow thruster, supply power of diesel generator, batteries, and ultra-capacitors.

IV. HIERARCHICAL CONTROL FOR IMPROVING ENERGY EFFICIENCY

According to the Fig.3, the principle of the coordinated control using hierarchical droop control for different supply sources is shown in Fig.4. The hierarchical droop control is employed for the paralleled energy storage system in which a power restoration control is used for the diesel generators in the second layer. In order to subdivide the fluctuations frequency of the bow thruster power cooperatively, a simple method is to insert the paired low-pass and high-pass filters into the droop controllers, thus the dynamic response speed of batteries and ultra-capacitors can follow the load fluctuations. However, the use of droop control results in a voltage drop of the converter DC bus and the voltage drop will make the diesel generator output power to change, therefore, a power restoration control is required, that is the secondary control which makes the output power of the diesel generator to be recovered to the average value of the thruster power, that is, move V_0 to adjust the reference voltage of the primary droop controller.

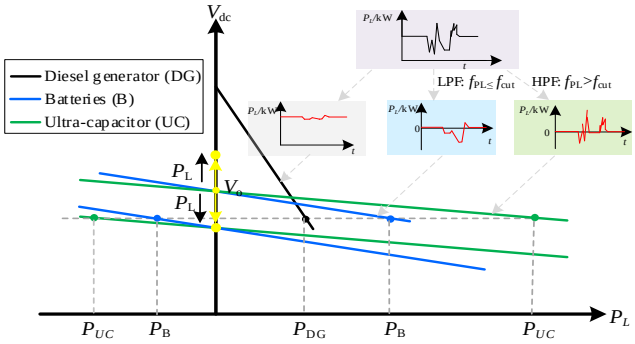

Fig. 4. Principle of the coordinated control among different supply sources.

A. Diesel generator and its speed regulator and exciter.

The mathematical model of six-cylinder four-stroke diesel engine is used [17]. The Fig.5 shows the speed control and excitation system of the diesel synchronous generator, in order to keep the output voltage and frequency stable.

The specific fuel consumption is the hourly consumption per unit of power, which is shown in the following equation [18].

$$SFC=C_0 / P_m + a + bP_m \quad (1)$$

where C_0, a, and b are the coefficients of the second-order polynomial function, and P_m is the mechanical power of the diesel engine.

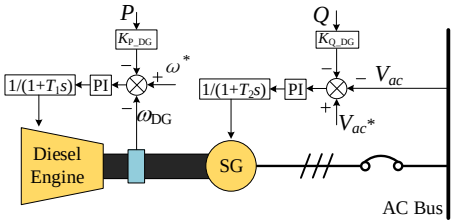

Fig. 5. DG and its speed regulator and exciter.

The synchronous generator passes through the three-winding transformer and 12-pulse rectification as shown in Fig. 6. The relationship between the output DC bus voltage V_{dc} and the output current I_{dc} is expressed in equation (2) [19], [20].

$$V_{dc} = \frac{3\sqrt{3}}{\pi} V_m - \frac{3}{\pi} \omega_e L_{ac} I_{dc} \tag{2}$$

Where V_m is the phase-voltage peak value of the synchronous generator, ω_e is the electrical angular speed, L_{ac} is the ac-side equivalent inductance, i.e., the synchronous inductance of the synchronous generator plus the sum of the primary and secondary leakage inductances of the three-winding transformer, and I_{dc} is the output DC current of the diesel generator. According to equation (2), the diesel generator with a rectifier exhibits the drooping characteristics, as shown in Fig. 4.

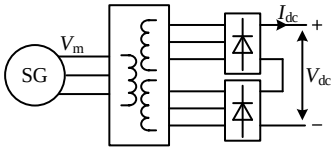

Fig. 6. The synchronous generator with three-winding transformer and 12-pulse rectifier.

B. A hierarchical droop control for the hybrid energy storage system.

Hierarchical droop control is provided shown in Fig.7. The primary control is to make the different-frequency load power sharing between the batteries and the ultra-capacitors. The secondary control is to make the output power of the diesel generator to be recovered to the reference value.

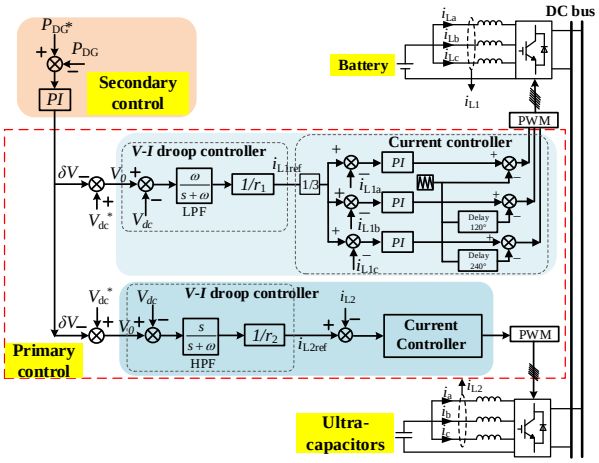

Fig. 7. Hierarchical control of DC/DC converters.

1)Primary control

A two-loop droop *V-I* controller is used for battery and ultra-capacitor converters that the *V-I* droop control with a low-pass/high-pass filters is the outer loop for different-frequency load power sharing and the inner loop is the current control for limiting the maximum discharging/charging current of the batteries. The droop gain is equivalent to a virtual resistance and the value of each virtual impedance can decide the current of energy storages.

The *V-I* droop control is formulated as:

$$i_{ref} = 1/r(V_{dc}^* - V_{dc}) \tag{3}$$

where r is the virtual resistance.

It can be also deformed into the following equation:

$$P_{con} = \frac{1}{m}(V_{dc}^* - V_{dc}) \tag{4}$$

where P_{con} *is the output power of the DC/DC converter*, m is the power droop coefficient, $m=r/V_{nom.}$, V_{nom} is the DC bus rated voltage. When $V_{dc} \approx V_{nom}$, $m=r/V_{dc}$.

Equation (4) reveals that the voltage deviation is determined by the output power of the supply sources and the virtual impedance.

The paired low-pass and high-pass filters (LPF and HPF) insert behind the voltage error of the voltage control loop that the load power fluctuations are subdivided into the low-frequency part and high-frequency part. The low-frequency load power can be balanced by the batteries and the high-frequency part can be made by the ultra-capacitors. The filter time constant is determined by the dynamic response speed of the batteries. From Table 1, we can choose 1Hz for the LPF and HPF.

2)Secondary control

The secondary control is for the output power restoration of the diesel generator. As shown in Fig. 4 and Fig.7, when the output power of the bow thruster changes, the DC bus voltage will fluctuate due to the droop characteristics. From equation (2), the output power of the diesel generator will follow the fluctuation of the DC bus voltage V_{dc}. A power loop with a *PI* controller is added to keep the output power of diesel generator constant.

By adding the active power compensation loop, a voltage deviation δV is added to the primary droop control. It can be formulated as follows,

$$P_{con} = \frac{1}{m}(V_{dc}^* - \delta V - V_{dc}) \tag{5}$$

When the output power of the diesel generator is not equal to the reference power P_{DG}^*, the secondary controller will change the $V_0 = V_{dc}^* - \delta V$ until the output power of the diesel generator is recovered.

C. Bow thruster control

The bow thruster generally uses the asynchronous machine. A rotor flux vector control method to attain the decoupled control of the flux and torque is used. The rotor flux is oriented in the d-axis of the rotating coordinate system, and the machine stator current is decomposed into an excitation component i_{sd} that generates the magnetic flux and a current torque component i_{sq} that controls the torque by the coordinate transformation.

According to the mathematical model of the asynchronous induction machine in the *dq0* coordinate system, the derivable magnetic chain and torque equations are as follows [21]:

$$\lambda_r = \frac{L_M}{T_r p + 1} i_{sd} \tag{6}$$

Where, $T_r=L_{rr}/r_r$, $L_{rr}=L_{lr}+L_M$, and L_{lr}, r_r are the rotor leakage inductance and resistance, L_M is the mutual inductance, p is the differential operator, i_{sd} is stator d-axis current, λ_r the rotor flux linkage.

$$T_e = \frac{3}{2}\frac{poles}{2}\frac{L_M}{L_{rr}}\lambda_r i_{sq} \tag{7}$$

Where T_e is the electrical torque, poles is The number of poles of the machine.

The slip angular velocity plus the rotor angular velocity, and after integral operation get the rotor flux position angle θ.

$$\theta = \int \omega dt = \int \left(\omega_r + \frac{r_r}{L_{rr}} \frac{L_M i_{sq}}{\lambda_r} \right) dt \tag{8}$$

A two-loop controller of the rotor flux vector control for the machine driver is shown in Fig. 8. The outer loop is the speed control and the inner loop is current control. The output of the outer-loop controller is the reference torque which can convert the reference torque current i_{sq} for the inner current loop according to equation (7). The flux reference currents i_{sd} is obtained by equation (5). Finally, the controller output is the three-phase modulation signal that controls the instantaneous frequency and voltage of the machine.

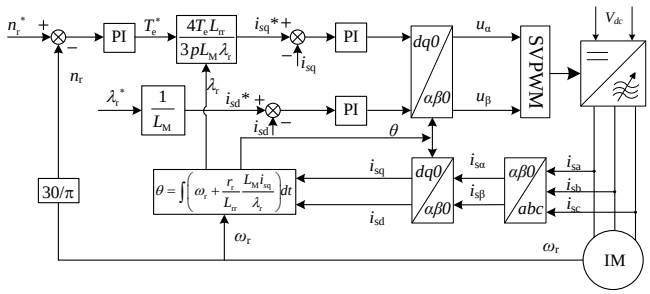

Fig. 8. Rotor flux vector control of the asynchronous machine.

The temperature is also an important factor affecting the performance, life and safety of shipboard microgrid. But this paper mainly focuses on the coordinated control method of the multiple power sources, and we supposed the temperature of the equipment in shipboard microgrid is controlled by the cooling system (such as water cooling, air cooling, etc.).

V. CONTROLLER PARAMETER DESIGN

If the droop control with a paired high/low-pass filters is only used for one DC/DC battery converter and another DC/DC UCs converter, the selection of droop coefficient is based on the required the output power of batteries/ UCs within the allowable voltage drop range, due to the addition of high/low-pass filters allows their response in complementary time scales. If multiple DC/DC converters parallel for batteries/ultra-capacitors, the droop coefficient, and its inner-loop parameters may cause the system instability. Furthermore, the system is more stable when the DC/DC converter parallels for batteries, due to the low-pass filter. Therefore, two paralleled DC/DC converters for UCs using droop control is analyzed.

The state space model of the bidirectional DC/DC converter with its droop controller can be expressed as follows:

$$\begin{cases} L\cdot\dfrac{d\hat{i}_L}{dt} = \hat{u}_B - D\cdot\hat{v}_{dc} + \hat{d}\cdot V_{dc} \\ C\cdot\dfrac{d\hat{v}_{dc}}{dt} = D\cdot\hat{i}_L - \hat{d}\cdot I_L - \hat{i}_o \\ \hat{i}_L^{\,*} = K\cdot(0-\hat{v}_{dc}) \\ \hat{d} = K_p(\hat{i}_L^{\,*} - \hat{i}_L) + K_i\int_0^t(\hat{i}_L^{\,*} - \hat{i}_L)dt \end{cases} \tag{9}$$

where L, C, D, V_{dc}, and I_L are the inductor, capacitor, steady-state duty ratio, steady-state DC bus voltage, and steady-state inductor current of the DC/DC converter. $\hat{i}_L$, $\hat{u}_B$, $\hat{v}_{dc}$, $\hat{d}$, and $\hat{i}_o$ are the state variables of the inductor current, the battery voltage, the bus voltage, the duty cycle, and the output current. The K, K_p, K_i are the virtual impedance coefficient of the outer loop *V-I* droop controller and the proportional and integral coefficient of the inner current loop *PI* controller.

When two DC/DC converters are connected in parallel, the state space equation can be expressed as follows:

$$\dot{x} = A\cdot x + B\cdot y \tag{10}$$

where $x=[\hat{I}_L \quad \hat{D} \quad \hat{v}_{dc}]'$ are the state variables, the column vector $\hat{I}_L=[\hat{i}_{L1} \quad \hat{i}_{L2}]'$ consisting of the state variables of the two converter inductor currents, $\hat{D}=[\hat{d}_1 \quad \hat{d}_2]'$ is the column vector composed of the state variables of the two converter duty cycles, $\hat{v}_{dc}$ is the state variable of the DC bus voltage. The input variable $y=[\hat{i}_{o1} \quad \hat{i}_{o2}]'$ is a column vector composed of the output current of the two converters. The state matrix A can be expressed as:

$$A=\begin{bmatrix} 0 & V_{dc}\cdot L^{-1} & -D\cdot L^{-1}\cdot I^T \\ -\dfrac{1}{C}\cdot K_p\cdot D\cdot K - K_i & \dfrac{1}{C}\cdot K_p\cdot I_L\cdot K - V_{dc}\cdot K_p\cdot L^{-1} & (D\cdot K_p\cdot L^{-1} - K_i\cdot K)\cdot I^T \\ I\cdot\dfrac{1}{C}\cdot D & -I\cdot\dfrac{1}{C}\cdot I_L & 0 \end{bmatrix} \tag{11}$$

and the output matrix B can be expressed as $B=[0 \quad \frac{1}{C}\cdot K_p\cdot K \quad -\frac{1}{C}]'$. Whereas V_{dc} is the steady-state value of the DC bus voltage. $D=\begin{bmatrix} D_1 & 0 \\ 0 & D_2 \end{bmatrix}$ $L=\begin{bmatrix} L_1 & 0 \\ 0 & L_2 \end{bmatrix}$ $I_L=\begin{bmatrix} I_{L1} & 0 \\ 0 & I_{L2} \end{bmatrix}$ are two-dimensional diagonal matrices consisting of duty cycle, inductors and inductor steady-state current of the DC/DC converter. $K_p=\begin{bmatrix} K_{p1} & 0 \\ 0 & K_{p2} \end{bmatrix}$ $K_i=\begin{bmatrix} K_{i1} & 0 \\ 0 & K_{i2} \end{bmatrix}$ $K=\begin{bmatrix} K_1 & 0 \\ 0 & K_2 \end{bmatrix}$ are two-dimensional diagonal matrices composed of the proportional and integral coefficient of the inner current loop *PI* controller and the droop control virtual impedance of all paralleled DC/DC converters $I=[1 \quad 1]$ is a 2-dimensional lateral vector.

When two paralleled DC/DC converters for UCs are connected in parallel with the same parameters of the current controller and the droop gains K=29, the current inner loop K_p=0.01, K_i=2, and the load power 150kW, the influence of the converter capacitance, the droop gain, the inner loop controller K_p and K_i on the system stability is shown in Fig. 9. From Fig. 9 (a), the system will be more stable when the DC bus capacitor increases. When this converter capacitor is too small, the system will be unstable. Considering the stability margin and response speed, the capacitor is chosen to be 8mF. When the droop gain K is changed, the root locus of the main eigenvalues is shown in Fig. 9(b). From Fig. 9 (b), when the droop gain is big, the system will be unstable. Fig. 9 (c) shows the system will be unstable when the inner-loop controller K_p is too small,

the system will be unstable. Fig. 9 (d) shows the system will be unstable when K_i is big.

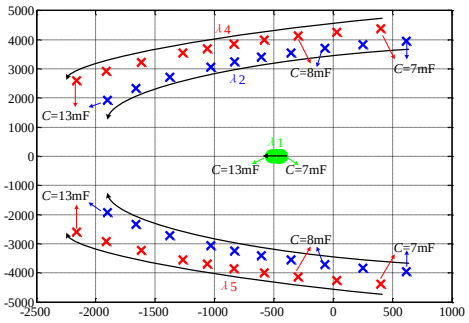

(a)The converter capacitance C changes

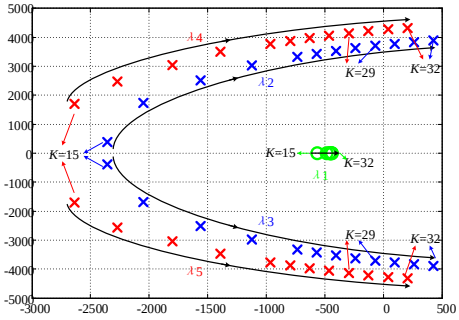

(b)The droop gain K changes

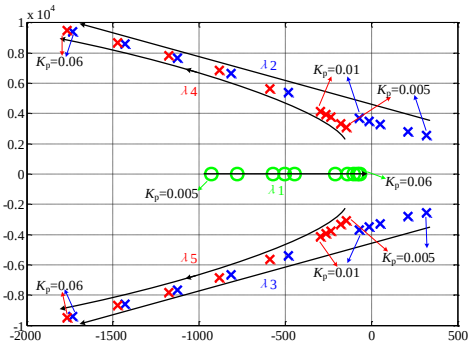

(c)The inner loop controller K_p changes

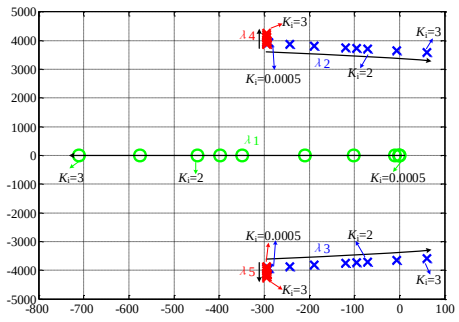

(d)The inner loop controller K_i changes

Fig. 9. Root locus plots of the main eigenvalue of the state-space model of the two paralleled DC/DC converters using droop control.

VI. SIMULATION RESULTS

The simulation model of a shipboard microgrid which the bow thruster supplied by diesel generator sets, batteries and UCs have implemented in Matlab/Simulink SimPowerSystems toolbox. The main parameters are shown in Table II, including the diesel engine, generator sets, speed regulator, exciter, induction machine of the bow thruster and its driver, batteries, battery DC/DC converter and its controller, UCs, and UCs DC/DC converter and its controller. The selected battery is a lithium-ion battery and the model can be found in [16].

TABLE II PARAMETERS OF A SHIPBOARD MICROGRID.

Battery	**Value**
Rated voltage of battery /V	550
Battery capacity /Ah	100
Maximum charge current /A	100
Maximum discharge current /A	120
Battery DC/DC converter and its controller	**Value**
The inductor of converter /mH	1
DC bus voltage /V	690
Switch frequency /kHz	10
V-I droop gain	3.6
Inner current loop PI controller K_p, K_i	0.01, 2
The cut-off frequency of Low pass filter /Hz	1
Power restoration loop PI controller K_p, K_i	1.5,10
Ultracapacitor	**Value**
Rated voltage of ultracapacitor /V	400
Ultracapacitor capacity /F	10
UC DC/DC converter and its controller	**Value**
The inductor of converter /mH	1
DC bus voltage	690
Switch frequency /kHz	10
V-I droop gain	28.8
Inner current loop PI controller K_p, K_i	0.01, 2
The cut-off frequency of High pass filter /Hz	1
Power restoration-loop PI controller K_p, K_i	1.5,10
Diesel engine	**value**
Number of engine cycles	4
Number of cylinders	6
Rated capacity /kVA	400
C_0 /(g/h)	12761.7
a /(g/kWh)	92.38
b /(g·kW/kWh))	0.235
Synchronous generator	**Value**
Nominal apparent power /kVA	400
RMS value of nominal phase to phase voltage /'	400
RMS value of nominal line current /A	577
Nominal frequency /Hz	50
Nominal speed /rpm	750
Pole pairs	4
d-axis synchronous reactance (X_d) /Ω	0.6066
d-axis transient reactance (X_d') /Ω	0.1317
d-axis subtransient reactance (X_d'') /Ω	0.0943
q-axis synchronous reactance (X_q) /Ω	0.1127
q-axis subtransient reactance (X_q'') /Ω	0.0163
Stator leakage reactance (X_l) /Ω	0.0113
d-axis transient time constant (T_{do}') /s	0.31
d-axis subtransient time constant (T_{do}'') /s	0.027
q-axis subtransient time constant (T_{qo}'') /s	0.01
Stator resistance (R_s) /Ω	0.09705
Inertia constant (H) /s	0.5006117
Speed regulator	**value**
PI controller	50, 0
The inertia time constant of the actuator /s	8e-5
Maximum fuel intake	0.9095
Minimum fuel intake	0.00544
Exciter	**value**
Rectifier smoothing time constant /s	0.002

Exciter time constant /s	0.002
Controller lead time constant /s	1.5
Controller lag time constant /s	1
Bow thruster and its driver	**value**
Rated power/kVA	150
RMS value of nominal phase to phase voltage /V	400 / 217
RMS value of nominal line current /A	50
Nominal frequency /Hz	
Pole pairs	2
Stator resistance /Ω	0.0293
Phase resistance of rotor winding /Ω	0.02026
Stator inductance /mH	0.2037
Rotor inductance /mH	0.2037
Stator and rotor mutual inductance /mH	3.738
Inertia constant /kg·m^2	5.79
Load torque/(N·m)	$1/3750\omega^2$
Rotor Flux linkage /Wb	0.73
Speed loop PI controller K_p, K_i	500, 600
Inner current PI controller K_p, K_i	5, 50

The rotor flux vector control method is used to control the asynchronous machine to simulate the quick start, short-time running and fast braking of the bow thruster. The simulation results are shown in Fig. 10. The speed change of the thruster machine is shown in Fig. 10(a). The output speed can follow the reference speed. Fig. 10 (b)-(c) show the output active/reactive power of the thruster machine. The active power and reactive power reach the maximum during the acceleration stage of the thruster machine. According to (6), the electromagnetic torque change of the thruster machine is shown in Fig. 10(d). As shown in Fig. 10 (e), the change of the stator current is as similar to the electromagnetic torque change. As can be seen from Fig. 10(b), (d) and (e), when the machine quickly brakes, it operates as a generator. Fig. 10(f) shows the excitation component of the stator current i_{ds}. When the rotor flux is controlled at a constant value of 0.73 Wb and the i_{ds} is equal to 300A. Therefore, this emulated asynchronous machine model can describe the characteristics of the bow thruster.

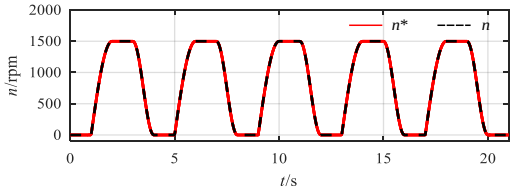

(a)The thruster machine speed reference and machine speed.

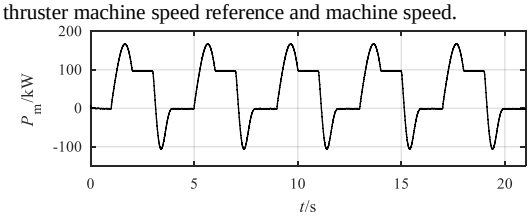

(b)The active power of thruster machine.

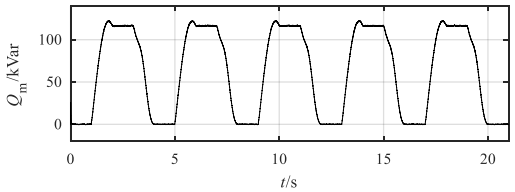

(c)The reactive power of the thruster machine.

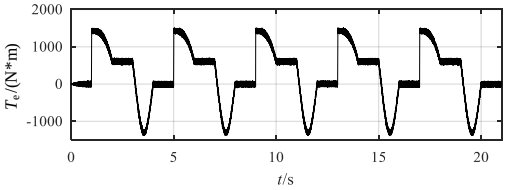

(d)Electromagnetic torque.

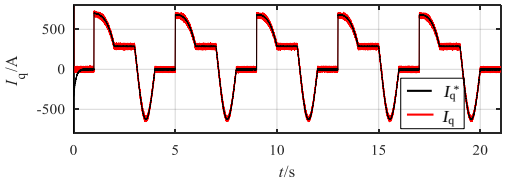

(e)The q-axis component of the thruster machine current.

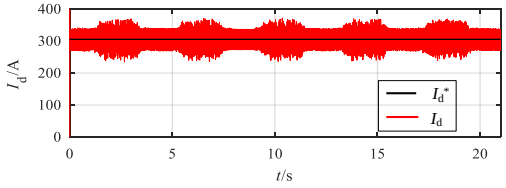

(f)The d-axis component of thruster machine current.

Fig. 10. Simulation results of the thruster machine.

The simulation results of multi-source supply for the bow thruster are shown in Fig. 11. Fig. 11(a) shows the power supplied to the bow thruster by the diesel generator, the batteries, and the UCs when the thruster power is changed. The thruster power is pulsating, and the average power of the bow thruster supplied by the diesel generator sets and it is almost constant. When the thruster power increases rapidly, the UC power follows it and then the battery output power increases. At this stage, the thruster power is provided by the diesel generator sets, the batteries and the UCs as shown in between 17s and 18s. When the thruster power remains unchanged, it is mainly provided by the batteries and the diesel generator as shown in between 16.5s and 17s. Between 19s and 19.5s, the speed of the bow thruster reduces rapidly, and the thruster machine is in the state of braking feedback operating as a generator. Therefore, the UCs quickly charge and track the power change of the thruster. Due to the battery charging process is electrochemically reaction and the response speed is relatively slow. The part energy of the rapidly changing power is stored in UCs, and the other is stored in the batteries.

The DC bus voltage of back-to-back converter and the AC bus voltage with and without the hybrid energy storages are shown in Fig.11(b) and (c). Since the control aim of the power restoration controller is to ensure that the power supplied by the diesel generator to the bow thruster unchanged, Fig. 11(b) shows the DC bus voltage of the thruster driver is in the required range, and it is controlled at 690V with the hybrid energy storages. The fluctuation of the DC bus voltage and the AC bus voltage are also decreased when the bow-thruster load power changes that can improve the stability of the shipboard microgrid.

Fig. 11(d) shows the required current of the thruster machine, the output current from the diesel generator, batteries and UCs to the bow thruster. It can be seen that the UC current rapidly increases and follows its required current. During the rapid braking, the thruster machine is operated as a generator. The

feedback current flows from the thruster machine into the UCs, which quickly charges.

When the machine speed is frequently changed, the voltage and SoC (state of charge) of the battery and the UCs, are shown in Fig. 11(e), (f), (g) and (h). The battery is always in a slight charge and discharge, effectively improving the battery life (cycle number). If the battery charge/discharge current is large, multiple sets of batteries may be connected in parallel by the DC/DC converters.

The comparison results of the SFC of the diesel engine and the output power from the diesel generator to the bow thruster with and without the hybrid energy storages are shown in Fig.11(i) and (j). With the hybrid energy storages, the diesel SFC remains stable and smaller, and also the output power from the diesel generator to the bow thruster is almost constant. Without the hybrid energy storages, the diesel SFC is bigger, and also the SFC and its output power to the bow thruster fluctuates with the power fluctuation of the bow thruster.

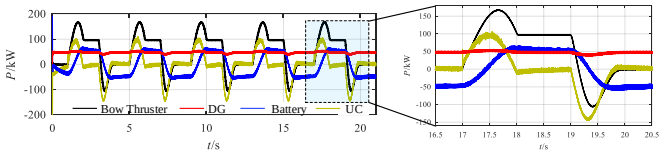

(a)The power of the thruster machine, DG, battery, and UC.

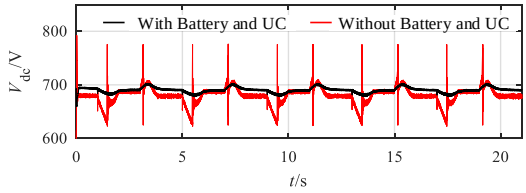

(b)DC bus voltage with and without hybrid energy storages.

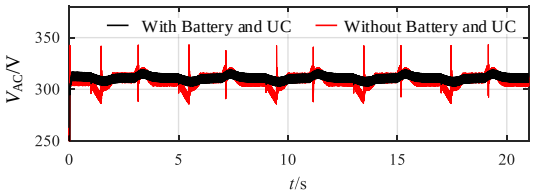

(c)AC bus voltage with and without hybrid energy storages.

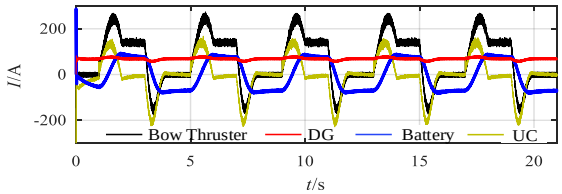

(d)The input current of the thruster machine, the output current of DG, battery, and UC.

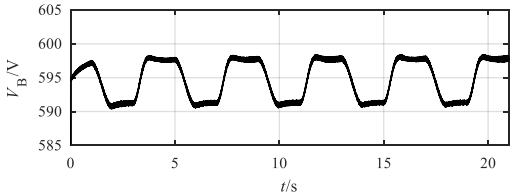

(e)Battery voltage

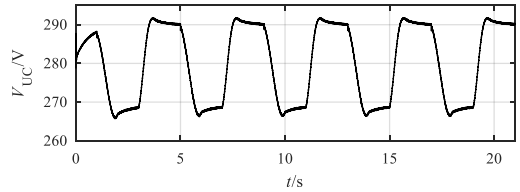

(f)UC voltage.

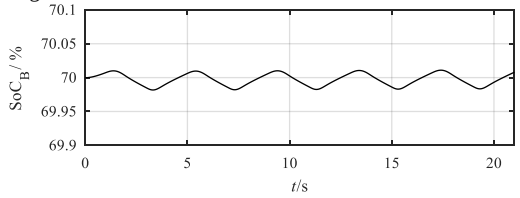

(g)Battery SoC.

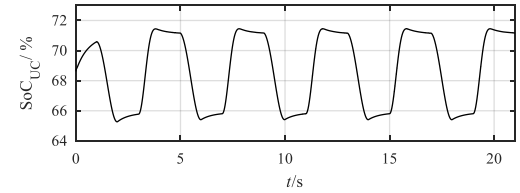

(h)UC SoC.

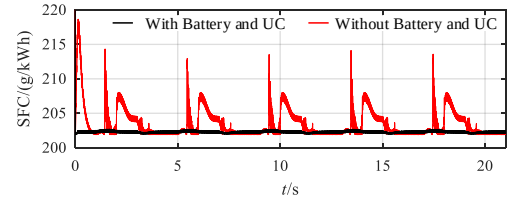

(i)Comparison of diesel SFC with and without hybrid energy storages.

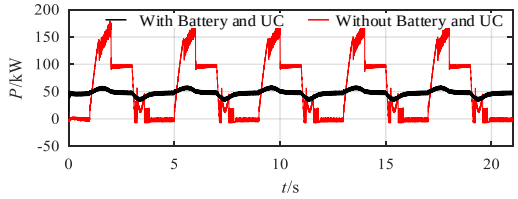

(j)Comparison of the diesel generator active power to the bow thruster with and without hybrid energy storages.

Fig.11. Simulation results of multi-source supply for the bow thruster.

In order to further verify the theoretical analysis results and the effectiveness of the proposed control strategy, a hardware-in-the-loop (HIL) simulation system is built and tested. consisting on a dSPACE platform, which encompasses a DS1006 processor board (based on a quad-core AMD Opteron™ x86 processor with 2.8 GHz clock frequency), digital I/O, A/D and D/A boards, and a host PC that uses ControlDesk as a user interface [22]. This experimental platform is shown in Fig.12 (a). The 18 SiC power modules with drivers is used to implement the two interleaved three-phase bidirectional DC/DC converters and the three-phase motor-driven inverter. The system is fully programmable from Matlab/Similink and the flowchart of HIL simulation sequence is shown in Fig. 12(b).

The hardware-in-the-loop results are shown in Fig.13. An induction motor is used to simulate the load power change of the electric propulsion by frequently starting, changing the rotation speed and stopping. An AC power source, batteries and ultracapacitors interfaced by the interleaved three-phase bidirectional DC/DC converters with the aforementioned

control scheme are used to meet the load power requirement of induction motor. The Fig.13 (a) shows the required current of the thruster machine, the output current from the diesel generator, batteries and UCs to the bow thruster when the thruster power is changed. And Fig.13 (b) shows the power supplied to the bow thruster by the diesel generator, the batteries, and the UCs. The hardware-in-the-loop results are the same as the simulation results, they all prove the correctness of the control strategy.

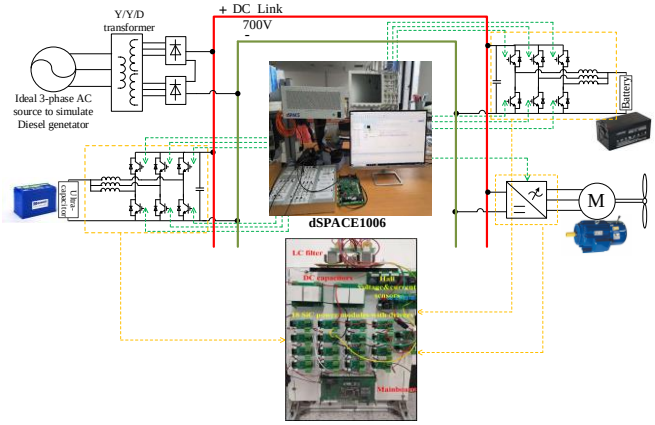

(a)Experimental platform

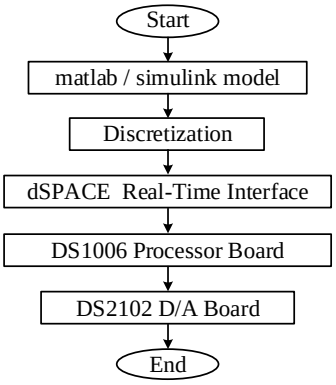

(b) The flowchart of hardware in the loop simulation.

Fig. 12. Experimental platform based on dSPACE1006 hardware-in-the-loop.

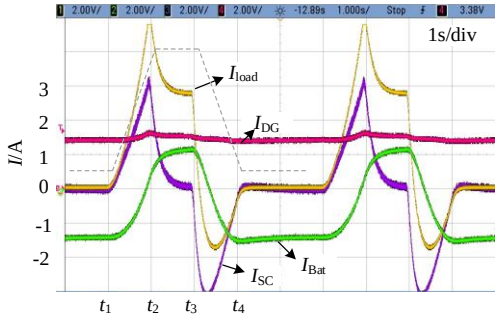

(a)Equivalent current (*I*):10A/div

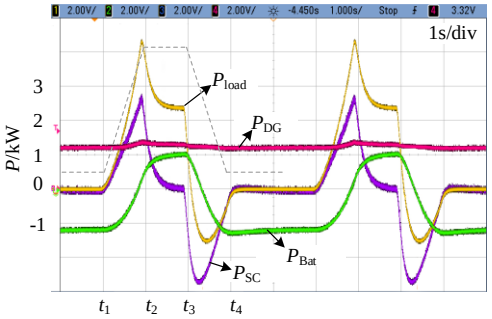

(b)Equivalent power (*P*):10kW/div

Fig. 13. Hardware-in-the-loop results of multi-source supply for the bow thruster.

VII. CONCLUSIONS

According to the operation states of the bow thruster in a ship, this paper proposes a hybrid power supply scheme that uses the UCs and batteries as a buffer to isolate the power fluctuations of the bow thruster from the shipboard microgrid. The UCs handle the high-frequency power fluctuations while the batteries deal with low-frequency power fluctuations of the bow thruster and the diesel generators provided the average power. A hierarchical controller is proposed to realize these functions and presents the following features:

- A *V-I* droop with high/low pass filters is in the primary control level to make the parallel operation of the storages and different time-scales power-sharing among them. Using this method, the power-sharing between UCs and batteries is according to the charge/discharge characteristics of different energy storages instead of their rated power or capacity characteristics.
- The power restoration control using the drooping characteristics of diesel generator with its rectification in the secondary level is proposed to realize the diesel-generator sets provide the required average power to the bow thruster and increases the energy efficiency of the diesel engines.
- This scheme can make the batteries in slight charge/discharge.

REFERENCES

[1] B. Zahedi, L. E. Norum, and K. B. Ludvigsen, "Optimized efficiency of all-electric ships by dc hybrid power systems," *Journal of Power Sources*, vol. 255, pp. 341-354, Jun 2014.

[2] E. K. Dedes, D. A. Hudson, and S. R. Turnock, "Assessing the potential of hybrid energy technology to reduce exhaust emissions from global shipping," *Energy Policy*, vol. 40, pp. 204-218, Jan 2012.

[3] E. Skjong, E. Rodskar, M. Molinas, T. A. Johansen, and J. Cunningham, " The Marine Vessel's Electrical Power System: From its Birth to Present Day," *Proceedings of the IEEE*, vol. 103, pp. 2410-2424, Dec 2015.

[4] S. Jayasinghe, L. Meegahapola, N. Fernando, Z. Jin, and J. Guerrero, "Review of ship microgrids: System architectures, storage technologies and power quality aspects," *Inventions*, vol. 2, p. 4, 2017.

[5] R. D. Geertsma, R. R. Negenborn, K. Visser, and J. J. Hopman, "Design and control of hybrid power and propulsion systems for smart ships: A review of developments," *Applied Energy*, vol. 194, pp. 30-54, May 15 2017.

[6] C. R. Lashway, A. T. Elsayed, and O. A. Mohammed, "Hybrid energy storage management in ship power systems with multiple pulsed loads," *Electric Power Systems Research*, vol. 141, pp. 50-62, Dec 2016.

[7] E. Skjong, R. Volden, E. Rodskar, M. Molinas, T. A. Johansen, and J. Cunningham, "Past, Present, and Future Challenges of the Marine Vessel's Electrical Power System," *IEEE Transactions on Transportation Electrification*, vol. 2, pp. 522-537, Dec 2016.

[8] R. D. Geertsma, R. R. Negenborn, K. Visser, and J. J. Hopman, "Design and control of hybrid power and propulsion systems for smart ships: A review of developments," *Applied Energy*, vol. 194, pp. 30-54, May 15 2017.
[9] W. Liu, J. M. Guerrero, M. Savaghebi, J. C. Vasquez, T. Tarasiuk, M. Gorniak, *et al.*, "Impact of the Voltage Dips in Shipboard Microgrid Power Systems," *IECON 2017 - 43rd Annual Conference of the IEEE Industrial Electronics Society*, ed, 2287-2292, 2017.
[10] L. Xing, et al. "Overview of current development in electrical energy storage technologies and the application potential in power system operation." Applied energy 137: 511-536,2015.
[11] A. Mohamed, V. Salehi, and O. Mohammed, "Real-Time Energy Management Algorithm for Mitigation of Pulse Loads in Hybrid Microgrids," *IEEE Transactions on Smart Grid*, vol. 3, pp. 1911-1922, Dec 2012.
[12] S. Kulkarni and S. Santoso, "Impact of pulse loads on electric ship power system: With and without flywheel energy storage systems," *2009 IEEE Electric Ship Technologies Symposium*, pp. 568-573, 2009.
[13] J. Moussodji and A. De Bernardinis, "Electric hybridization of a bow thruster for river boat application," *2015 IEEE Transportation Electrification Conference and Expo (ITEC)*, pp. 1-6, 2015,
[14] Z. Jin, L. Meng, J. M. Guerrero, and R. Han, "Hierarchical Control Design for a Shipboard Power System With DC Distribution and Energy Storage Aboard Future More-Electric Ships," *IEEE Transactions on Industrial Informatics*, vol. 14, pp. 703-714, Feb 2018.
[15] J. Hou, J. Sun, and H. F. Hofmann, "Mitigating Power Fluctuations in Electric Ship Propulsion With Hybrid Energy Storage System: Design and Analysis," *IEEE Journal of Oceanic Engineering*, vol. 43, pp. 93-107, Jan 2018.
[16] K. Kim, K. Park, G. Roh, and K. Chun, "DC-grid system for ships: a study of benefits and technical considerations," *Journal of International Maritime Safety, Environmental Affairs, and Shipping*, vol. 2, pp. 1-12, 2018.
[17] P. M. Anderson and M. Mirheydar, "Analysis of a diesel-engine driven generating unit and the possibility for voltage flicker," *IEEE Transactions on Energy Conversion*, vol. 10, no. 1, pp. 37-47, March 1995.
[18] Zahedi B, Norum L E, Ludvigsen K B. Optimized efficiency of all-electric ships by dc hybrid power systems[J]. Journal of power sources, 2014, 255: 341-354.
[19] S. Sudhoff, S. Pekarek, S. Glover, S. Zak, E. Zivi, J. Sauer, *et al.*, "Stability analysis of a dc power electronics based distribution system," SAE Technical Paper 0148-7191, 2002.
[20] A. Di Gerlando, G. M. Foglia, M. F. Iacchetti, and R. Perini, "Comprehensive steady-state analytical model of a three-phase diode rectifier connected to a constant DC voltage source," *Iet Power Electronics*, vol. 6, pp. 1927-1938, Nov 2013.
[21] P. C. Krause, O. Wasynczuk, and S. D. Sudhoff, *Analysis of Electric Machinery and Drive Systems.* Piscataway, NJ: IEEE Press, 2002.
[22]
[23] dSPACE1006 User Manual:
https://www.dspace.com/shared/data/pdf/2019/dSPACE_DS1006_Catalog2019.pdf

Zhao-xia Xiao received the B.S. degree in Electrical Engineering and Automation, Hebei University of Technology, the M.S. degree in Control Theory and Control Engineering, and the Ph.D. degree in Power System and its Automation from Tianjin University, Tianjin, P. R. China, in 2002, 2005 and 2008, respectively. From 2007-2008, she studied in University of Manchester, UK as a Ph.D. Guest. Since 2009, she began to work in Tianjin Polytechnic University. She has been an associate professor and full professor from 2011,2018. From Sep. 2012 to Dec. 2012 she was a Visiting Scholar in Fraunhofer IWES, Germany. From Dec.2016 to Jan.2018, she was a Visiting Scholar in Department of Energy Technology, Aalborg University, Denmark. Her research interests include AC/DC Microgrids with renewable energy, maritime microgrids, planning of distribution network. She has authored and co-authored more than 30 technical papers in Microgrids journals and conferences.

Huai-min Li received the B.S. degree in electrical engineering and automation from University of Jinan, Jinan, China, in 2017. He is currently working toward the M.S. degree in electrical engineering from Tiangong University, Tianjin, China.
His research interests include control of power electronic converters, DC microgrids, and their applications in maritime microgrids.

Hong-wei Fang was born in Anhui, China, in 1977. He received the B. S. degree, the M. S. and Ph.D. from Tianjin University, China, in 1999, 2004, and 2007 respectively, all in electrical engineering. From Oct. 2009 to Dec. 2009, he was a visitor fellow in Universitat Politècnica de Catalunya, Barcelona, Spain.
He is currently an associate professor in the School of Electrical and Information Engineering, Tianjin University, China. His current research interests include electrical machines & drives, power electronics, wind and ocean wave energy power generation. Dr. Fang's awards and honors include IEEE senior member, the peer reviewer of IEEE Transactions on Industrial Electronics, IEEE Transactions on Power Electronics, IEEE Transactions on Energy Conversion, etc.

Yu-zhe Guan received the B.S. degree in automation from Xiangtan University, Xiangtan, China, in 2017. He is currently working toward the M.S. degree in electrical engineering fromTiangong University, Tianjin, China.
His research interests include control of power electronic converters, DC microgrids, and their applications in maritime microgrids.

Tao Liu was born in Hebei, China, in 1984. He received the B.S. degree, M.S. degree and Ph.D. degree in electrical engineering from Tianjin University, Tianjin, China in 2008, 2010 and 2014.
He is currently a Lecturer with the School of Electrical Engineering and Automation, Tianjin Polytechnic University. He is engaged in the research on motor and drive in Tianjin Key Laboratory of Advanced Technology of Electrical Engineering and Energy.
His research interests include permanent magnet synchronous motor drive system, grid-connected converter, and power quality.

Lucas Hou received his Ph.D. degree in Electrical Engineering from Xi'an Jiaotong University, Xi'an, P. R. China, in 2003. He Worked as deputy chief engineer in Chengdu Dongfang Kaiqi Electric Co., Ltd from Jan. of 2004 to Nov. of 2004. He Worked as chief engineer in Guangdong Mingyang Longyuan Power Electronics Co., Ltd from Dec. of 2004 to Jun. of 2006. He Worked as chief engineer in Guangdong Mingyang Wind Power Technology Co., Ltd from Jun. of 2006 to Feb. of 2008. He is the chairman in REnergy Electric Tianjin LTD from Mar. of 2008 to now.
Lucas Hou has been engaged in the power electronics and new energy industries for decades, and has obtained more than 20 patents. As the project leader, he has led more than 20 national and provincial and municipal science and technology projects including the national key new products, the national "863" smart microgrid project, and the major training project of Tianjin science and technology giants leading enterprises , which won the first prize of Tianjin Science and Technology Progress Award in 2016. As one of the first level talents of Tianjin "131" innovative talent training project, he was selected as the leader in Tianjin "131" innovative talent team. In 2019, he was appraised by the State Council Special Allowance Expert.

Josep M. Guerrero (S'01-M'04-SM'08-FM'15) received the B.S. degree in telecommunications engineering, the M.S. degree in electronics engineering, and the Ph.D. degree in power electronics from the Technical University of Catalonia, Barcelona, in 1997, 2000 and 2003, respectively. Since 2011, he has been a Full Professor with the Department of Energy Technology, Aalborg University, Denmark, where he is

The final version of record is available at http://dx.doi.org/10.1109/TTE.2020.2992735

responsible for the Microgrid Research Program. From 2014 he is chair Professor in Shandong University; from 2015 he is a distinguished guest Professor in Hunan University; and from 2016 he is a visiting professor fellow at Aston University, UK, and a guest Professor at the Nanjing University of Posts and Telecommunications. From 2019, he became a Villum Investigator by The Villum Fonden, which supports the Center for Research on Microgrids (CROM) at Aalborg University, being Prof. Guerrero the founder and Director of the same centre (www.crom.et.aau.dk).

His research interests are oriented to different microgrid aspects, including power electronics, distributed energy-storage systems, hierarchical and cooperative control, energy management systems, smart metering and the internet of things for AC/DC microgrid clusters and islanded minigrids. Specially focused on microgrid technologies applied to offshore wind, maritime microgrids for electrical ships, vessels, ferries and seaports, and space microgrids applied to nanosatellites and spacecrafts. Prof. Guerrero is an Associate Editor for a number of IEEE TRANSACTIONS. He has published more than 500 journal papers in the fields of microgrids and renewable energy systems, which are cited more than 50,000 times. He received the best paper award of the IEEE Transactions on Energy Conversion for the period 2014-2015, and the best paper prize of IEEE-PES in 2015. As well, he received the best paper award of the Journal of Power Electronics in 2016. During six consecutive years, from 2014 to 2019, he was awarded by Clarivate Analytics (former Thomson Reuters) as Highly Cited Researcher. In 2015 he was elevated as IEEE Fellow for his contributions on “distributed power systems and microgrids.”